



Implementation of Haar wavelet, higher order Haar wavelet, and differential quadrature methods on buckling response of strain gradient nonlocal beam embedded in an elastic medium

Subrat Kumar Jena¹ · S. Chakraverty¹ · Mohammad Malikan^{2,3}

Received: 21 August 2019 / Accepted: 26 October 2019 / Published online: 9 November 2019
© Springer-Verlag London Ltd., part of Springer Nature 2019

Abstract

The present investigation is focused on the buckling behavior of strain gradient nonlocal beam embedded in Winkler elastic foundation. The first-order strain gradient model has been combined with the Euler–Bernoulli beam theory to formulate the proposed model using Hamilton’s principle. Three numerically efficient methods, namely Haar wavelet method (HWM), higher order Haar wavelet method (HOHWM), and differential quadrature method (DQM) are employed to analyze the buckling characteristics of the strain gradient nonlocal beam. The impacts of several parameters such as nonlocal parameter, strain gradient parameter, and Winkler modulus parameter on critical buckling loads are studied effectively. The basic ideas of the numerical methods, viz. HWM, HOHWM, and DQM are presented comprehensively. Also, a comparative study has been conducted to explore the effectiveness and applicability of all the three numerical methods in terms of convergence study. Finally, the results, obtained by this investigation, are validated properly with other works published earlier.

Keywords Buckling behavior · Strain gradient model · Nonlocal beam · HWM · HOHWM · DQM

1 Introduction

Nowadays, numerical methods and algorithms have come to help the engineers and researchers to open the way for solving complex scientific problems such as molecular structural analysis, meteorology and weather forecasting, system dynamics, and many other essential topics. In general, numerical calculations use the practical results of computing to find new ways to analyze problems. In engineering

problems, the analysis of structures using modern numerical methods is one of the most widely used problems [1].

More recently, the mechanical and structural analyses of nanostructures due to their widespread applications with the help of modern numerical methods has received much attention [2–25]. Among these numerical methods, the Haar wavelet method [26–28] and higher order Haar wavelet method [29, 30] and also differential quadrature method [31–33] are among the advanced numerical methods with excellent precision. The wavelet is a special series of functions that are now known as the first wavelet. This series was presented as the simplest type of the wavelet first introduced by Alfred Haar in 1909. Mathematically, the wavelet is a set of fixed piece functions that can approximate a function. Among the published papers, Hein and Feklistova [34] investigated Haar wavelets to study free vibrations of non-uniform and axially functionally graded beams under different boundary conditions. They transformed their equations based on the simplest wavelets. Their results were appropriately matched with the other presented works. Lepik [35] based on the Euler–Bernoulli beam model studied an elastic local beam containing a crack subjected to a longitudinal in-plane load based on the Haar wavelet method. His results proved the high accuracy of the Haar wavelet method. Kirs

✉ S. Chakraverty
sne_chak@yahoo.com

Subrat Kumar Jena
sjena430@gmail.com

Mohammad Malikan
mohammad.malikan@yahoo.com

¹ Department of Mathematics, National Institute of Technology Rourkela, Rourkela 769008, India

² Department of Mechanics of Materials and Structures, Faculty of Civil and Environmental Engineering, Gdansk University of Technology, Gdansk, Poland

³ Department of Mechanical Engineering, Faculty of Engineering, Islamic Azad University, Mashhad Branch, Mashhad, Iran

et al. [36] analyzed dynamically a nonlocal Euler–Bernoulli beam model based on the Haar wavelets. They also carried out three boundary conditions, namely pinned–pinned, clamped–clamped, and clamped–pinned ones.

As it has been seen so far, the properties of materials such as their energy at the nanoscale vary with their large-scale state. However, the size reduction is a physical change, and it is not expected that the basic properties of the material will change with this physical change. This has made the nanoscale more attractive than other scales. Properties such as electrical conductivity, color, mechanical strength, and even weight can be changed at the nanoscale. For example, the conductivity of metals is well known. However, metals can be a semiconductor or even insulated on a nanoscale. Nanomaterials also have a much higher surface-to-volume ratio compared to bulk materials. This is a fundamental property that is extremely important in all processes that occur on the surface of the material (such as reactivity). So it can be stated that nano does not just mean a thousand times smaller than micro. Investigating the mechanical behavior of a nanostructure at the nanoscale is in dire need of a suitable theory that to date elasticity theory of nonlocal of Eringen [37–42], couple stress [43, 44] and strain gradient theories [45–49] predict the behavior of nanostructures extensively as a mechanical analysis under different conditions. However, in this study, the size-dependent effects have been described employing the nonlocal strain gradient theory, which is a combination of the Eringen’s nonlocal theory and the second-order Mindlin strain gradient theory, which can well show the effects of size reduction and atomic interaction [50, 51].

More recently, some researchers have focused on the main model of nonlocal strain gradient theory, namely its integral forms [52, 53]. As a matter of fact, both nonlocal and strain gradient terms instead of their differential models have been re-considered in their integral models. They have found that in some beam analyses, the results of differential models may be inconsistent with the integral ones’ results. In addition, in some valuable researches [54, 55], researchers have presented that while considering nonlocal elasticity theory of Eringen or nonlocal strain gradient approach, there have been more appropriate numerical outcomes if the effect of change in the thickness is investigated in the gradients of stress and strain, that is, although the effect of changes in the thickness has been ignored in the strains by researchers, the effect of size-dependent can be crucial in the thickness direction. Of some important conclusions within these studies, they showed that the thickness effect strengthens the effect of nonlocal strain gradient theory and by ignoring the effect of thickness the stiffness-hardening effect is underestimated. In fact, the stiffness-hardening and stiffness-softening influences are affected by the length to thickness ratio when considering the thickness effect.

This research has come to consider profoundly and comprehensively various advanced numerical approaches, namely Haar wavelet method (HWM), higher order Haar wavelet method (HOHWM) and differential quadrature method (DQM) to analyze a nanobeam under mechanical stability situation. To this, the classical beam model is embedded in the energy formulation to extract the equilibrium equations and the strain gradient nonlocal model reformulates the obtained local equations to implement a nanoscale behavior in the problem. Moreover, the Winkler elastic matrix is assumed to be as an outer effect. Afterward, several diagrams are graphically plotted with the results of the HWM, HOHWM, and DQM for two boundary conditions, namely pinned–pinned and clamped–clamped ones to show the stability behavior of the modeled nanobeam.

2 Review of the strain gradient model

The stress field as per the first-order nonlocal strain gradient model [19, 50–68] is presented as

$$\sigma_{xx} = \sigma_{xx}^\diamond - \nabla \sigma_{xx}^* \tag{1}$$

where $\sigma_{xx}^\diamond = \int_0^L E\alpha(x, x', e_0a) \epsilon'_{xx}(x') dx'$ and

$$\sigma_{xx}^* = l^2 \int_0^L E\alpha^*(x, x', e_1a) \epsilon'_{xx,x}(x') dx'$$

denote the classical nonlocal stress tensor and the higher order nonlocal stress tensor, respectively. $\alpha(x, x', e_0a)$ and $\alpha^*(x, x', e_1a)$ are the nonlocal kernel, ϵ_{xx} and $\epsilon_{xx,x}$ represent the strain and gradient of strain, L and l are the length of nanobeam and material length-scale parameter, and e_0a , and e_1a are the nonlocal parameters due to the higher order strain gradient stress field. Applying the nonlocal differential operator ($\ell_i = 1 - (e_i a)^2 \nabla^2, i = 0, 1$) on the stress field, viz. Eq. (1), the first-order strain gradient model for a one-dimensional elastic material is described as [53]

$$\begin{aligned} & \left(1 - (e_0a)^2 \frac{\partial^2}{\partial x^2}\right) \left(1 - (e_1a)^2 \frac{\partial^2}{\partial x^2}\right) \sigma_{xx} \\ & = E \left(1 - (e_1a)^2 \frac{\partial^2}{\partial x^2}\right) \epsilon_{xx} - El^2 \left(1 - (e_0a)^2 \frac{\partial^2}{\partial x^2}\right) \frac{\partial^2}{\partial x^2} \epsilon_{xx}. \end{aligned} \tag{2}$$

Considering $e_0 = e_1$, Eq. (2) is converted into [50–68]:

$$\left(1 - (e_0a)^2 \frac{\partial^2}{\partial x^2}\right) \sigma_{xx} = E \left(1 - l^2 \frac{\partial^2}{\partial x^2}\right) \epsilon_{xx}. \tag{3}$$

3 Formulation of proposed model

The displacement field of the Euler–Bernoulli beam at any point may be defined as [37]

$$u_1(x, z, t) = u(x, t) - z \frac{\partial w(x, t)}{\partial x}, \tag{4a}$$

$$u_2(x, z, t) = 0, \tag{4b}$$

$$u_3(x, z, t) = w(x, t), \tag{4c}$$

where u_1 , u_2 , and u_3 represent displacements along x , y , and z directions, respectively, whereas $u(x, t)$ and $w(x, t)$ denote axial and transverse deflections of the point on the mid-plane of the beam. Using von Kármán hypothesis, the nonlinear strain–displacement relation may be expressed as

$$\varepsilon_{xx} = \frac{\partial u(x, t)}{\partial x} - z \frac{\partial^2 w(x, t)}{\partial x^2} + \frac{1}{2} \left(\frac{\partial w(x, t)}{\partial x} \right)^2. \tag{5}$$

Hamilton’s principle for the conservative system is presented as

$$\delta \prod = \int_{t_1}^{t_2} \delta (W_e + U) dt, \tag{6}$$

where U is the strain energy and W_e is the work done by the elastic foundation. The variations in strain energy and external work done are given as

$$\delta U = \int_0^L \int_A \sigma_{xx} \delta \varepsilon_{xx} dA dx = \int_0^L \left[N_{xx} \frac{\partial \delta u}{\partial x} - M_{xx} \frac{\partial^2 \delta w}{\partial x^2} + N_{xx} \frac{\partial w}{\partial x} \frac{\partial \delta w}{\partial x} \right] dx, \tag{7}$$

$$\delta W_e = - \int_0^L k_w w \delta w dx, \tag{8}$$

where k_w is the Winkler modulus, σ_{xx} is the normal stress, $N = \int_A \sigma_{xx} dA$, and $M = \int_A \sigma_{xx} z dA$ are axial force and bending moment, respectively. Substituting Eqs. (7) and (8) in Eq. (6) and setting $\delta \prod = 0$, we have

$$\delta \prod = \int_0^t \int_0^L \left[N_{xx} \frac{\partial \delta u}{\partial x} - M_{xx} \frac{\partial^2 \delta w}{\partial x^2} + N_{xx} \frac{\partial w}{\partial x} \frac{\partial \delta w}{\partial x} - k_w w \delta w \right] dx dt = 0. \tag{9}$$

On simplification of Eq. (9) and taking $N_{xx} = P$, the constitutive relation may be derived as

$$\frac{\partial^2 M_{xx}}{\partial x^2} - P \frac{\partial^2 w}{\partial x^2} - k_w w = 0. \tag{10}$$

Multiplying Eq. (3) by $z dA$ and integrating over A , we have

$$M_{xx}^{nl} = (e_0 a)^2 \frac{\partial^2 M}{\partial x^2} - EI \frac{\partial^2 w}{\partial x^2} + I^2 EI \frac{\partial^4 w}{\partial x^4}, \tag{11}$$

where e_0 and a denote material constant and internal characteristic length, respectively, $I = \int_A z^2 dA$ is the second moment of inertia and E is Young’s modulus. Inserting Eq. (10) in Eq. (11), the nonlocal bending moment M_{xx}^{nl} can be changed into

$$M_{xx}^{nl} = (e_0 a)^2 \left(P \frac{\partial^2 w}{\partial x^2} + k_w w \right) - EI \frac{\partial^2 w}{\partial x^2} + I^2 EI \frac{\partial^4 w}{\partial x^4}. \tag{12}$$

Putting Eq. (12) in Eq. (10), and assuming $w(x, t) = w_0(x) \sin \omega t$, the governing equation is given as

$$(e_0 a)^2 k_w \frac{d^2 w_0}{dx^2} + (e_0 a)^2 P \frac{d^4 w_0}{dx^4} - EI \frac{d^4 w_0}{dx^4} + I^2 EI \frac{d^6 w_0}{dx^6} - P \frac{d^2 w_0}{dx^2} - k_w w_0 = 0, \tag{13}$$

Now, using $X = \frac{x}{L}$, $W = \frac{w_0}{L}$, $K_w = \frac{k_w L^4}{EI}$, $\hat{P} = \frac{PL^2}{EI}$ and $\beta = \frac{l}{L}$ in Eq. (13), the normalizing form of governing equation may be derived as

$$\beta^2 \frac{d^6 W}{dX^6} - \frac{d^4 W}{dX^4} + \frac{(e_0 a)^2}{L^2} K_w \frac{d^2 W}{dX^2} - K_w W = \hat{P} \left(\frac{d^2 W}{dX^2} - \frac{(e_0 a)^2}{L^2} \frac{d^4 W}{dX^4} \right). \tag{14}$$

4 Preliminaries

4.1 Haar wavelet

The Haar function can be expressed as [28–30, 35, 36, 69, 70]

$$h_i(x) = \begin{cases} 1 & \text{for } x \in [\phi_1(i), \phi_2(i)] \\ -1 & \text{for } x \in [\phi_2(i), \phi_3(i)] \\ 0 & \text{elsewhere} \end{cases}, \tag{15}$$

where $i = m + k + 1$, where $m = 2^j$ and k denote the maximum number of square waves and the position of the particular square wave in the interval $[I_1, I_2]$. Also, $\phi_1(i) = I_1 + k \frac{I_2 - I_1}{2^j}$, $\phi_2(i) = I_1 + (2k + 1) \frac{I_2 - I_1}{2^{j+1}}$, and $\phi_3(i) = I_1 + (k + 1) \frac{I_2 - I_1}{2^j}$, where $j(j = 0, 1, \dots, J)$ and $k(k = 0, 1, \dots, 2^j - 1)$ represent the dilatation and translation parameters of the wavelets, respectively. J is termed as maximal of resolution of the wavelets. The Haar function, presented in Eq. (15) is only valid if $i \geq 2$. For $i = 1$, $h_1(x) = 1$ for $x \in [I_1, I_2]$ and 0 elsewhere.

The κ th integral of the Haar function (for $i > 1$), presented in Eq. (1) can be derived analytically as [28–30, 35, 36, 69, 70]

$$p_{\kappa,i}(t) = \frac{1}{\kappa!} \begin{cases} 0 & \text{for } x \in [I_1, \phi_1(i)) \\ (x - \phi_1(i))^\kappa & \text{for } x \in [\phi_1(i), \phi_2(i)) \\ (x - \phi_1(i))^\kappa - 2(x - \phi_2(i))^\kappa & \text{for } x \in [\phi_2(i), \phi_3(i)) \\ (x - \phi_1(i))^\kappa - 2(x - \phi_2(i))^\kappa + (x - \phi_3(i))^\kappa & \text{for } x \in [\phi_3(i), I_2) \end{cases} \quad (16)$$

For $i = 1$, we have $\phi_1 = I_1$, $\phi_2 = \phi_3 = I_2$ and $p_{\eta,1}(t) = \frac{1}{\eta!}(t - S)^\eta$.

The collocation points are considered as [29, 35, 70]

$$x_k = I_1 + (k - 0.5) \frac{I_2 - I_1}{2^{J+1}}, \quad k = 1, 2, \dots, 2^{J+1}. \quad (17)$$

$H, P_1, P_2, P_3, \dots, P_\kappa$ are the Haar matrices of dimension 2^{J+1} and the elements of these matrices are expressed by $H(i, k) = h_i(x_k)$ and $P_\kappa(i, k) = p_{\kappa,i}(x_k)$.

4.2 Differential quadrature method

In the present investigation, Quan and Chang’s [71, 72] version of Differential Quadrature Method has been implemented. According to this approach, the derivatives of any function $W(X)$ at a given discrete point i can be expressed as linear sums of functions at discrete grid points, which are demonstrated as [31–33]

$$W'_i = \sum_{j=1}^N A_{ij} W_j, \quad (18a)$$

$$W''_i = \sum_{j=1}^N B_{ij} W_j, \quad (18b)$$

$$W'''_i = \sum_{j=1}^N C_{ij} W_j, \quad (18c)$$

$$W_i^{IV} = \sum_{j=1}^N D_{ij} W_j, \quad (18d)$$

$$W_i^V = \sum_{j=1}^N E_{ij} W_j, \quad (18e)$$

$$W_i^{VI} = \sum_{j=1}^N F_{ij} W_j, \quad (18f)$$

where $A_{ij}, B_{ij}, C_{ij}, D_{ij}, E_{ij}$ and F_{ij} are the weighting coefficient matrices, and N is the number of discrete grid points. Chebyshev–Gauss–Lobatto grid points have been used in this

study which is defined as [31–33]

$$X_i = \frac{1}{2} \left[1 - \cos \left(\frac{i-1}{N-1} \cdot \pi \right) \right]. \quad (19)$$

The weighting coefficient matrices can be computed using Lagrange interpolation by the following procedure [31–33].

For $i \neq j$,

$$A_{ij} = \frac{1}{X_j - X_i} \prod_{\substack{k \neq i \\ k=1 \\ k \neq j}}^N \frac{X_i - X_k}{X_j - X_k} \quad i = 1, 2, \dots, N \quad j = 1, 2, \dots, N \quad (20a)$$

for $i = j$

$$A_{ii} = \sum_{\substack{k \neq i \\ k=1}}^N \frac{1}{X_i - X_k} \quad i = 1, 2, \dots, N. \quad (20b)$$

Other weighting coefficients of higher order derivatives can be produced by performing matrix multiplications as [31–33]

$$B = B_{ij} = \sum_{k=1}^N A_{ik} A_{kj}, \quad (21)$$

$$C = C_{ij} = \sum_{k=1}^N A_{ik} B_{kj}, \quad (22)$$

$$D = D_{ij} = \sum_{k=1}^N A_{ik} C_{kj} = \sum_{k=1}^N B_{ik} B_{kj}, \quad (23)$$

$$E = E_{ij} = \sum_{k=1}^N A_{ik} D_{kj} = \sum_{k=1}^N B_{ik} C_{kj}, \quad (24)$$

$$F = F_{ij} = \sum_{k=1}^N A_{ik} E_{kj} = \sum_{k=1}^N B_{ik} D_{kj} = \sum_{k=1}^N C_{ik} C_{kj}. \quad (25)$$

5 Implementation of HWM, HOHWM, and DQM in the proposed model

For the investigation of buckling behavior of stain gradient nonlocal beam, pinned–pinned (P–P), and clamped–clamped (C–C) boundary conditions are taken into consideration which is given as [58]

Pinned–pinned (P–P):

$$W(0) = 0, \frac{d^2W}{dX^2}(0) = 0, \frac{d^4W}{dX^4}(0) = 0$$

$$\text{and } W(1) = 0, \frac{d^2W}{dX^2}(1) = 0, \frac{d^4W}{dX^4}(1) = 0. \tag{26}$$

Clamped–clamped (C–C):

$$W(0) = 0, \frac{dW}{dX}(0) = 0, \frac{d^3W}{dX^3}(0) = 0$$

$$\text{and } W(1) = 0, \frac{dW}{dX}(1) = 0, \frac{d^3W}{dX^3}(1) = 0. \tag{27}$$

5.1 Haar wavelet method

According to HWM, the highest order derivative of the governing equation, viz. $\frac{d^6W}{dX^6}$ in Eq. (14) can be expressed as [35, 36]

$$\frac{d^6W}{dX^6} = \sum_{i=1}^N c_i h_i = C^T H, \tag{28}$$

where $N = 2^{J+1}$. Performing sixth-time integration successively, we have

$$\frac{d^5W}{dX^5}(X) = C^T P_1(X) + d_1, \tag{29a}$$

$$\frac{d^4W}{dX^4}(X) = C^T P_2(X) + d_1 X + d_2, \tag{29b}$$

$$\frac{d^3W}{dX^3}(X) = C^T P_3 + d_1 \frac{X^2}{2} + d_2 X + d_3, \tag{29c}$$

$$\frac{d^2W}{dX^2}(X) = C^T P_4 + d_1 \frac{X^3}{6} + d_2 \frac{X^2}{2} + d_3 X + d_4, \tag{29d}$$

$$\frac{dW}{dX}(X) = C^T P_5 + d_1 \frac{X^4}{24} + d_2 \frac{X^3}{6} + d_3 \frac{X^2}{2} + d_4 X + d_5 \tag{29e}$$

$$W(X) = C^T P_6 + d_1 \frac{X^5}{120} + d_2 \frac{X^4}{24} + d_3 \frac{X^3}{6} + d_4 \frac{X^2}{2} + d_5 X + d_6 \tag{29f}$$

Here $c = (c_1, c_2, c_3, \dots, c_N)^T$ and $d_1, d_2, d_3, d_4, d_5,$ and d_6 are integration constants which are different for particular boundary conditions. Substituting Eq. (29) with proper boundary condition, the governing Eq. (14) will be converted into an Eigenvalue problem as

$$[K]\{C\} = \hat{P}[B]\{C\}, \tag{30}$$

where the Eigenvalue \hat{P} is the buckling load parameter.

Theorem 1 *Let us assume a square-integrable, finite function $\varphi(x) = \frac{d^r \phi(x)}{dx^r}$ in the interval $[0, 1]$ and $\exists \kappa$ such that $|\frac{d\varphi(x)}{dx}| \leq \kappa$, for all $x \in [0, 1]$, then the HWM based on the discretized approach is convergent and the order of convergence is computed as two.*

Proof For the proof, one may see an interesting paper [73].□

5.2 Higher order haar wavelet method

From Theorem 1, it is found that the order of convergence of HWM is two. To improve the order of convergence, Majak et al. [30] proposed another approach. According to this technique, we have

$$\frac{d^{n+2\tau}W}{dX^{n+2\tau}} = C^T H, \quad \tau = 1, 2, \dots, \tag{31}$$

where n is the highest order derivative and τ is the extra term which is going to enhance the order of convergence of HOHWM. Assigning $\tau = 1, n + 2$ integration constants will be generated and the extra two integration constants can be handled using the algorithm presented in [30, 74].

Now setting $\tau = 1$ and following the procedures of HOHWM, we obtain

$$\frac{d^8W}{dX^8} = \sum_{i=1}^N c_i h_i = C^T H. \tag{32}$$

Integrating successively, we get

$$\frac{d^6W}{dX^6} = C^T P_2(X) + d_1 X + d_2, \tag{33a}$$

$$\frac{d^5W}{dX^5}(X) = C^T P_3(X) + d_1 \frac{X^2}{2} + d_2 X + d_3, \tag{33b}$$

$$\frac{d^4W}{dX^4}(X) = C^T P_4(X) + d_1 \frac{X^3}{6} + d_2 \frac{X^2}{2} + d_3 X + d_4, \tag{33c}$$

$$\frac{d^3W}{dX^3}(X) = C^T P_5(X) + d_1 \frac{X^4}{24} + d_2 \frac{X^3}{6} + d_3 \frac{X^2}{2} + d_4 X + d_5, \tag{33d}$$

$$\frac{d^2W}{dX^2}(X) = C^T P_6(X) + d_1 \frac{X^5}{120} + d_2 \frac{X^4}{24} + d_3 \frac{X^3}{6} + d_4 \frac{X^2}{2} + d_5 X + d_6, \tag{33e}$$

$$\frac{dW}{dX}(X) = C^T P_7(X) + d_1 \frac{X^6}{720} + d_2 \frac{X^5}{120} + d_3 \frac{X^4}{24} + d_4 \frac{X^3}{6} + d_5 \frac{X^2}{2} + d_6 X + d_7, \tag{33f}$$

$$W(X) = C^T P_8(X) + d_1 \frac{X^7}{5040} + d_2 \frac{X^6}{720} + d_3 \frac{X^5}{120} + d_4 \frac{X^4}{24} + d_5 \frac{X^3}{6} + d_6 \frac{X^2}{2} + d_7 X + d_8, \tag{33g}$$

Here $C = (c_1, c_2, c_3, \dots, c_N)^T$ and $d_1, d_2, d_3, d_4, d_5, d_6, d_7$ and d_8 are integration constants. Out of these eight constants, six can be obtained from each of the boundary condition, presented in Eqs. (26) and (27) whereas the rest two can also be obtained from the governing equation as

$$\beta^2 \frac{d^6W}{dX^6}(0) - \frac{d^4W}{dX^4}(0) + \frac{(e_0 a)^2}{L^2} K_w \frac{d^2W}{dX^2}(0) - K_w W(0) = \hat{P} \left(\frac{d^2W}{dX^2}(0) - \frac{(e_0 a)^2}{L^2} \frac{d^4W}{dX^4}(0) \right), \tag{34}$$

$$\beta^2 \frac{d^6W}{dX^6}(1) - \frac{d^4W}{dX^4}(1) + \frac{(e_0 a)^2}{L^2} K_w \frac{d^2W}{dX^2}(1) - K_w W(1) = \hat{P} \left(\frac{d^2W}{dX^2}(1) - \frac{(e_0 a)^2}{L^2} \frac{d^4W}{dX^4}(1) \right). \tag{35}$$

Plugging Eq. (31) in governing Eq. (14) and performing the procedures properly as mentioned in [30, 74], governing Eq. (14) will be converted into a generalized Eigenvalue problem as Eq. (30) where the Eigenvalues represent the buckling load parameters.

5.3 Differential quadrature method

Applying Eqs. (21–25) in Eqs. (26–27), the pinned–pinned (P–P) and clamped–clamped (C–C) boundary conditions are given as [19]

Pinned–pinned:

$$\begin{aligned} \{W'\} &= [\bar{A}]\{W\} \\ \{W''\} &= [A]\{W'\} = [A][\bar{A}]\{W\} = [\bar{B}]\{W\} \\ \{W'''\} &= [\bar{A}]\{W''\} = [\bar{A}][\bar{B}]\{W\} = [\bar{C}]\{W\} \\ \{W^{IV}\} &= [A]\{W'''\} = [A][\bar{C}]\{W\} \\ &= [\bar{B}][\bar{B}]\{W\} = [\bar{D}]\{W\} \\ \{W^V\} &= [\bar{A}]\{W^{IV}\} = [\bar{A}][\bar{D}]\{W\} \\ &= [\bar{A}][\bar{B}][\bar{B}]\{W\} = [\bar{E}]\{W\} \\ \{W^{VI}\} &= [A]\{W^V\} = [A][\bar{E}]\{W\} \\ &= [A][\bar{A}][\bar{B}][\bar{B}]\{W\} = [A][\bar{A}][\bar{D}]\{W\} = [\bar{F}]\{W\}. \end{aligned}$$

Clamped–clamped:

$$\begin{aligned} \{W'\} &= [\bar{A}]\{W\} \\ \{W''\} &= [\bar{A}]\{W'\} = [\bar{A}][\bar{A}]\{W\} = [\bar{B}]\{W\} \\ \{W'''\} &= [A]\{W''\} = [A][\bar{B}]\{W\} = [\bar{C}]\{W\} \\ \{W^{IV}\} &= [\bar{A}]\{W'''\} = [\bar{A}][\bar{C}]\{W\} = [\bar{D}]\{W\} \\ \{W^V\} &= [A]\{W^{IV}\} = [A][\bar{D}]\{W\} \\ &= [A][\bar{A}][\bar{C}]\{W\} = [\bar{E}]\{W\} \\ \{W^{VI}\} &= [A]\{W^V\} = [A][\bar{E}]\{W\} \\ &= [A][A][\bar{A}][\bar{C}]\{W\} = [\bar{F}]\{W\}, \end{aligned}$$

in which A, \bar{A}, \bar{A}_1 and \bar{A}_2 are given as

$$\begin{aligned} A &= \begin{bmatrix} A_{11} & A_{12} & \dots & A_{1,N-1} & A_{1,N} \\ A_{21} & A_{22} & \dots & A_{2,N-1} & A_{2,N} \\ \vdots & \vdots & & \vdots & \vdots \\ A_{N1} & A_{N2} & \dots & A_{N,N-1} & A_{N,N} \end{bmatrix} \\ \bar{A} &= \begin{bmatrix} 0 & A_{12} & \dots & A_{1,N-1} & 0 \\ 0 & A_{22} & \dots & A_{2,N-1} & 0 \\ \vdots & \vdots & & \vdots & \vdots \\ 0 & A_{N2} & \dots & A_{N,N-1} & 0 \end{bmatrix} \\ \bar{A}_1 &= \begin{bmatrix} 0 & A_{1,2} & \dots & A_{1,N} \\ 0 & A_{2,2} & \dots & A_{2,N} \\ \dots & \dots & \dots & \dots \\ 0 & A_{N,2} & \dots & A_{N,N} \end{bmatrix} \\ \bar{A}_2 &= \begin{bmatrix} A_{1,1} & A_{1,2} & \dots & A_{1,N-1} & 0 \\ A_{2,1} & A_{2,2} & \dots & A_{2,N-1} & 0 \\ \dots & \dots & \dots & \dots & \dots \\ A_{N,1} & A_{N,2} & \dots & A_{N-1,N-1} & 0 \end{bmatrix}. \end{aligned}$$

Substituting Eq. (18) along with the above boundary conditions in Eq. (14), a generalized Eigenvalue problem will be formed.

6 Numerical results and discussion

Governing Eq. (14) has been solved by HWM, HOHWM, and DQM as an Eigenvalue problem using MATLAB codes developed by the authors. The critical buckling load parameter (\hat{P}_{cr}) also has been obtained for pinned–pinned and clamped–clamped boundary conditions with $E = 1$ TPa, $L = 10$ nm, and $h = 1$ nm.

6.1 Validation

The critical buckling loads, obtained by HWM, HOHWM, and DQM for both the PP and CC boundary conditions are validated with Wang et al. [75] assigning $K_w = 0$ and $\beta = 0$

whereas other parameters remain same as Wang et al. [75]. The comparisons of results are given in a graphical form which is illustrated in Fig. 1. The graphical results are drawn by varying the nonlocal parameter (e_0a) from 0 to 2 with an increase of 0.5. From Fig. 1, it is revealed that the results obtained by present methods are showing a decent agreement with the reference.

6.2 Convergence study

Convergence studies are carried out for all the three methods, viz. HWM, HOHWM, and DQM concerning the critical buckling load. In this regard, pinned–pinned boundary condition has been considered for the study. The critical buckling loads are calculated with $e_0a = 0.5$, $K_w = 50$, $\beta = 0.2$, and $L = 20$. For HWM, the convergence is attained at $J = 5$ whereas, for HOHWM, the same results are obtained at $J = 2$. In the case of DQM, the results start converging at $N = 8$ or $J = 2$. These investigations are noted in Table 1

Fig. 1 Validation of present results with [75]

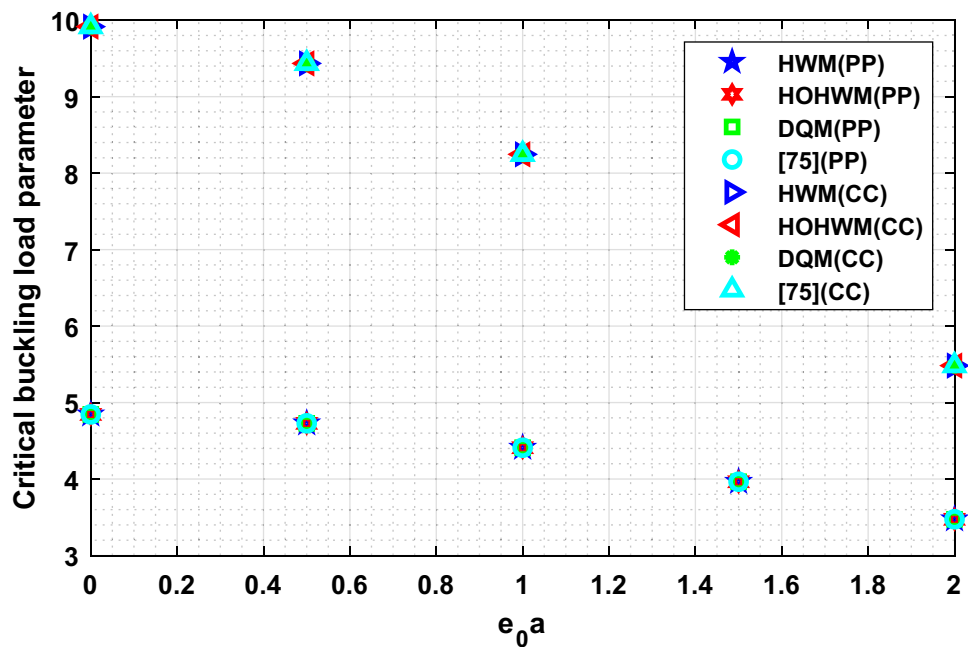


Table 1 Convergence of critical buckling load parameter (\hat{P}_{cr}) by HWM, HOHWM, and DQM with $e_0a = 0.5$, $K_w = 50$, $\beta = 0.2$ and $L = 20$ for pinned–pinned (P–P) boundary condition

J	$N = 2^{J+1}$	HWM	HOHWM	DQM	o (HWM)	o (HOHWM)
1	4	2.314765	2.301424	2.430377	–	–
2	8	2.303851	2.300723	2.300684	–	–
3	16	2.301451	2.300683	2.300680	2.1851	4.1364
4	32	2.300871	2.300680	2.300680	2.0503	4.0345
5	64	2.300728	2.300680	2.300680	2.0128	4.0086
6	128	2.300692	2.300680	2.300680	2.0032	4.0021
7	256	2.300683	2.300680	2.300680	2.0008	4.0005
8	512	2.300681	2.300680	2.300680	2.0002	4.0000

Fig. 2 Convergence study of HWM, HOHWM, and DQM

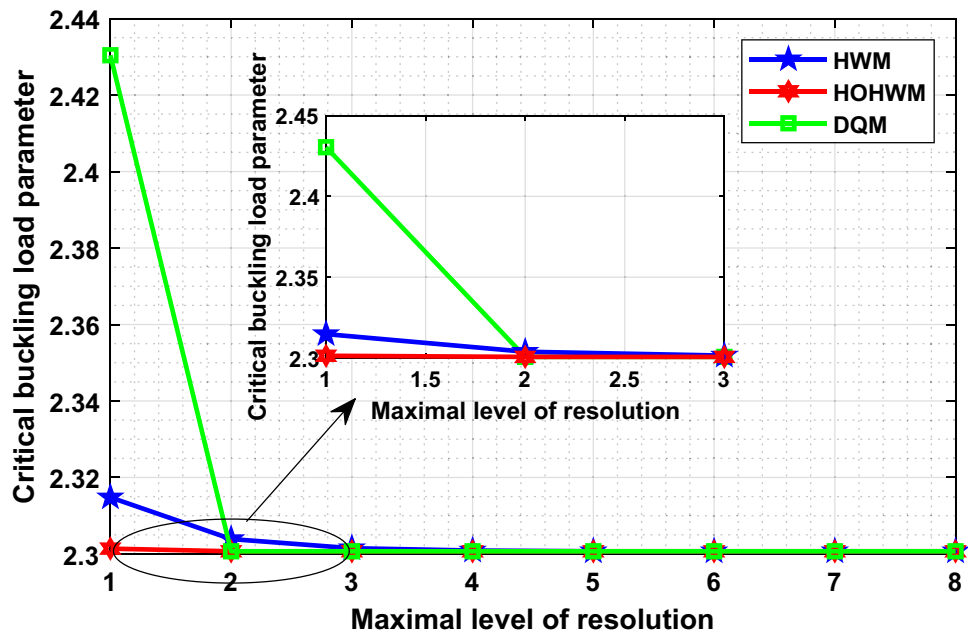


Table 2 Effect of e_0a on critical buckling load parameter (\hat{P}_{cr}) and critical buckling load ratio by HWM, HOHWM and DQM with $K_w = 100$, $\beta = 0.1$ and $L = 10$

e_0a	Pined–pined		Clamped–clamped	
	\hat{P}_{cr}	Critical load ratio	\hat{P}_{cr}	Critical load ratio
0	10.2965	1.0000	30.7494	1.0000
0.5	10.1683	0.9875	28.0985	0.9138
1	9.8183	0.9536	22.3967	0.7284
1.5	9.3292	0.9061	16.8676	0.5486
2	8.7899	0.8537	12.6817	0.4124
2.5	8.2657	0.8028	9.7509	0.3171
3	7.1799	0.6973	7.7219	0.2511
3.5	5.8748	0.5706	6.2973	0.2048
4	4.9377	0.4796	5.2743	0.1715

and Fig. 2. Also, the order of convergence for HWM and HOHWM are calculated based on the formula presented in [76], and it is found that the order of convergence is approximately two and four, respectively. It may also be noted that HOHWM converges as fast as DQM exhibiting its supremacy over HWM.

6.3 Effect of nonlocal parameter

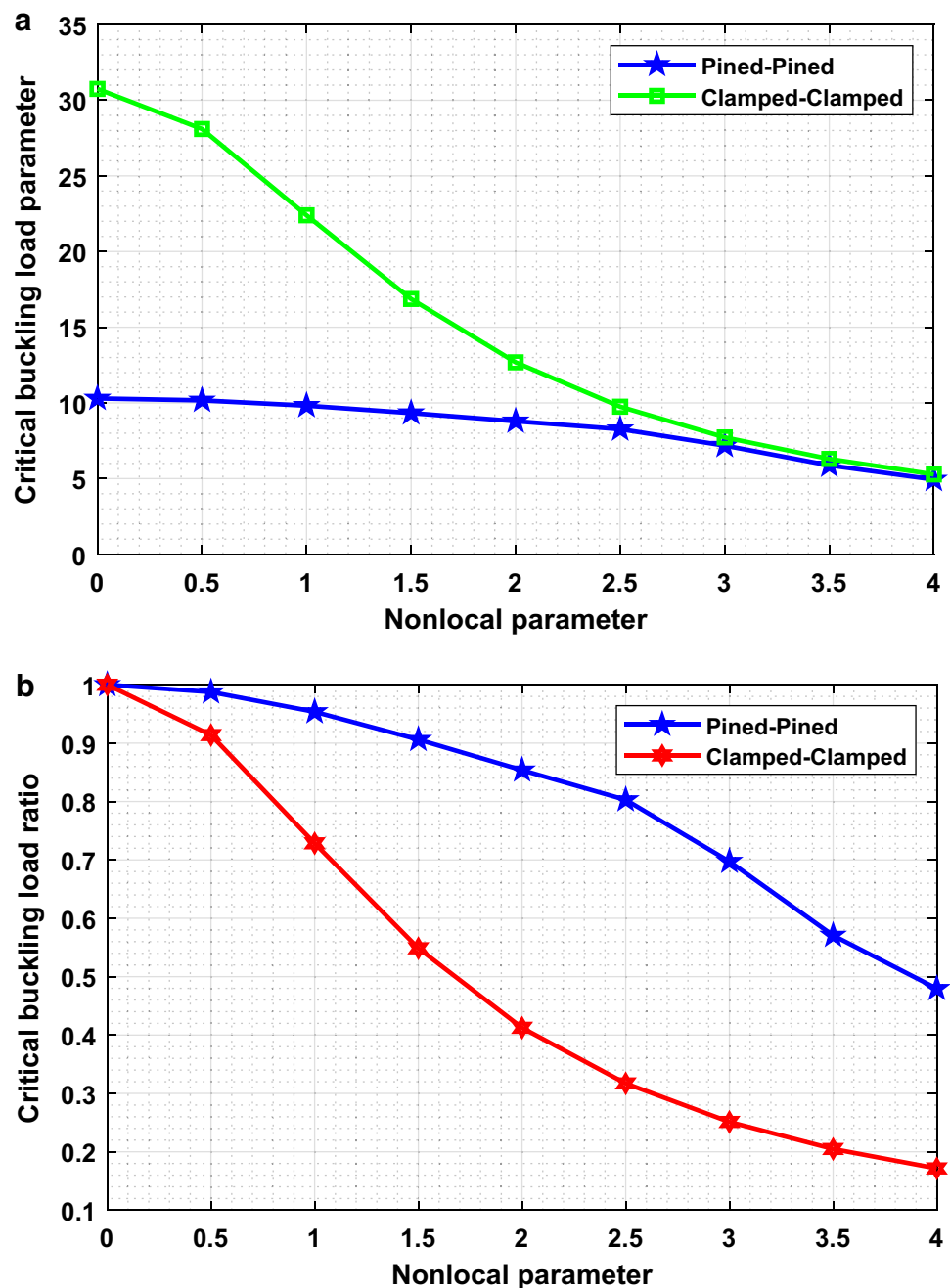
The impacts of nonlocal parameters (e_0a) are noted on the critical buckling load (\hat{P}_{cr}) and critical buckling load ratio

in forms of tabular result and graphical plot. The critical buckling load ratio is defined as the ratio of critical buckling load parameter using nonlocal theory and critical buckling load parameter using classical theory. The results are calculated with $K_w = 100$, $\beta = 0.1$ and $L = 10$. Also, $J = 8$ for HWM, $J = 4$ for HOHWM, and $N = 25$ for DQM are taken in the computation. The nonlocal parameters (e_0a) are varying from 0 to 4 with an increment of 0.5. The results are demonstrated in Table 2 and Figs. 3 and 4. From these results, it is observed that the critical buckling load parameters are decreasing with an increase of (e_0a) for both the boundary conditions and this reduction in critical buckling load is more significant in case of clamped–clamped boundary condition.

6.4 Effect of strain gradient parameter

In this subsection, the response of the strain gradient parameter (β) on critical buckling load (\hat{P}_{cr}) has been noted with $K_w = 200$, and $L = 10$. Critical buckling loads are calculated for different nonlocal parameters (e_0a) by varying strain gradient parameter from 0 to 1 with an increment of 0.2. Critical buckling loads increase with the increase of strain gradient parameters, but this increase is much faster in case of clamped–clamped boundary conditions, which can be illustrated in Table 3 and Figs. 4 and 5. Also, critical buckling load is maximum in the case of classical theory with higher values of strain gradient parameters, and this trend is equal for both the boundary conditions.

Fig. 3 **a** Critical buckling load versus nonlocal parameter, **b** critical buckling load ratio versus nonlocal parameter



6.5 Effect of Winkler modulus parameter

The impacts of Winkler modulus parameters (K_w) on critical buckling loads are studied through this subsection. The results are computed with $e_0a = 1$, and $L = 10$ by HOW, HOHWM, and DQM by considering $J = 8$, $J = 4$, and $N = 20$, respectively. Both the boundary conditions such as PP and CC are considered for the study by changing K_w from 0 to 500 with an increase of 100 for different values of strain gradient parameters. Both the graphical and tabular results are presented in Figs. 6 and 7, and Table 4. From

these results, it can be concluded that the increase of Winkler modulus parameter increases the critical buckling load for both the boundary conditions. Also, this increases much higher in CC boundary condition with higher values of strain gradient parameters.

6.6 Buckling mode shape

Buckling mode shape is essential to predict the buckling characteristics of structural members. In this regard, mode shapes are plotted by considering the PP boundary

Fig. 4 Critical buckling load versus strain gradient parameter for PP case

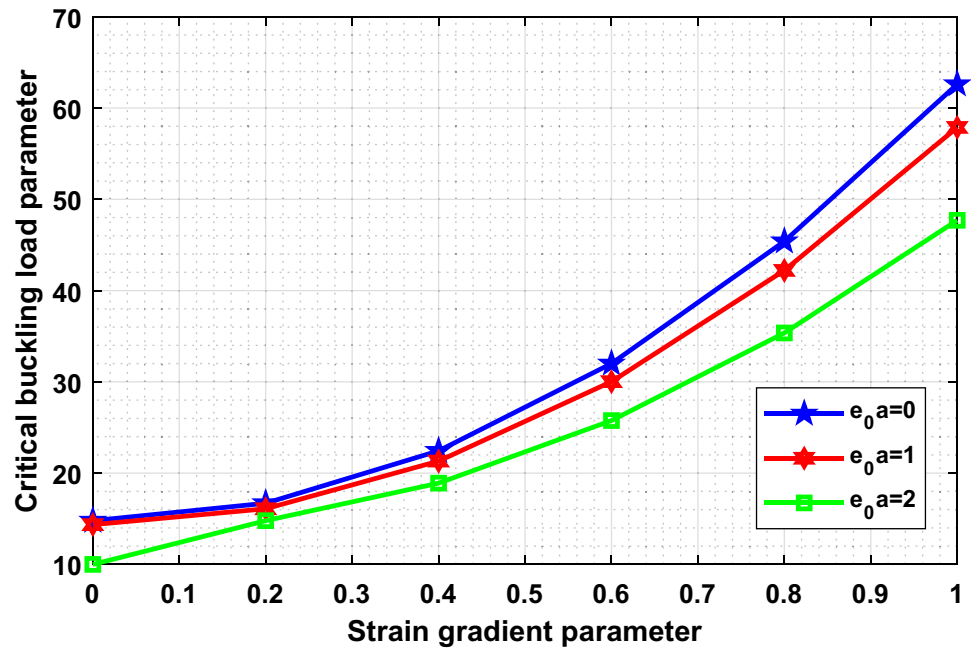


Table 3 Effect of β on critical buckling load parameter (\hat{P}_{cr}) by HWM, HOHWM, and DQM with $K_w = 200$, and $L = 10$

β	Pinned–pinned			Clamped–clamped		
	$\hat{P}_{cr}(e_0 a = 0)$	$\hat{P}_{cr}(e_0 a = 1)$	$\hat{P}_{cr}(e_0 a = 2)$	$\hat{P}_{cr}(e_0 a = 0)$	$\hat{P}_{cr}(e_0 a = 1)$	$\hat{P}_{cr}(e_0 a = 2)$
0	14.7919	14.3567	10.0005	26.6948	19.7635	10.7700
0.2	16.7045	16.0975	14.7919	57.4281	41.8764	23.7876
0.4	22.4424	21.3200	18.9057	149.2444	107.7055	59.3884
0.6	32.0055	30.0240	25.7621	302.2572	217.4091	118.7157
0.8	45.3939	42.2097	35.3609	516.4730	370.9927	201.7729
1	62.6075	57.8770	47.7024	791.8928	568.4567	308.5605

Fig. 5 Critical buckling load versus strain gradient parameter for CC case

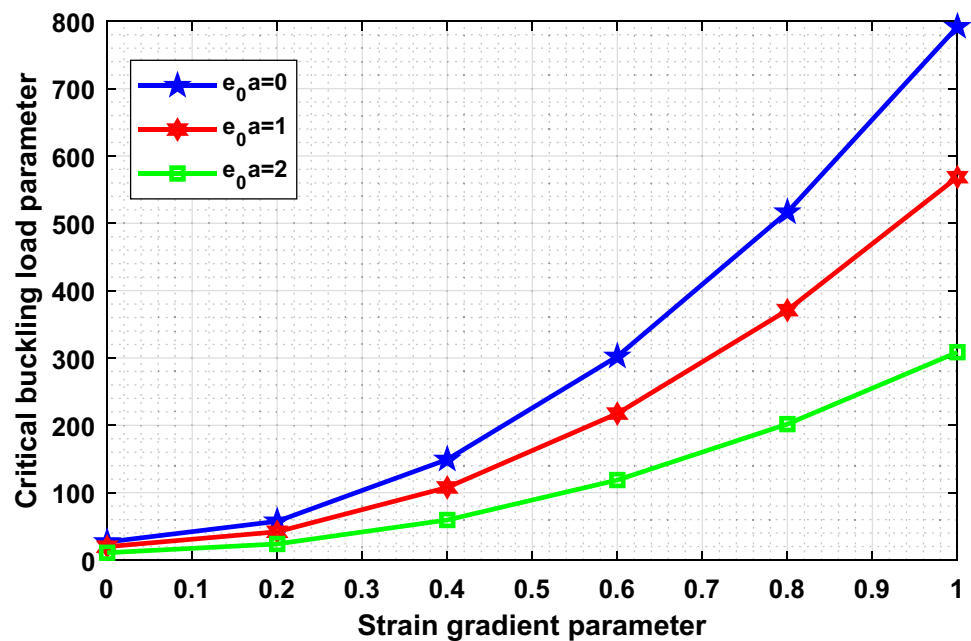


Fig. 6 Critical buckling load versus Winkler modulus parameter for PP case

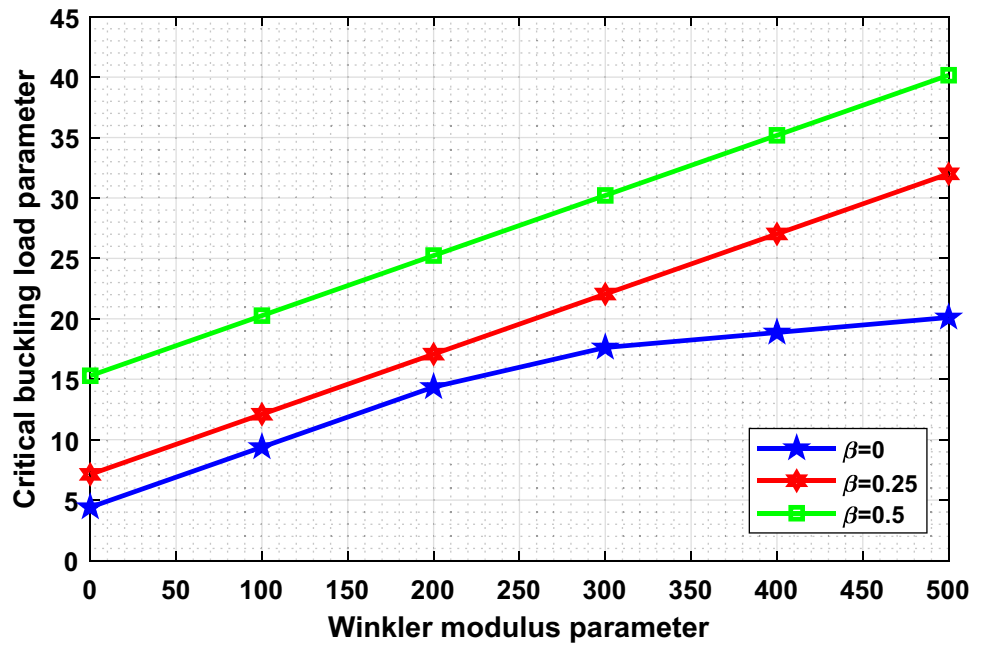


Fig. 7 Critical buckling load versus Winkler modulus parameter for CC case

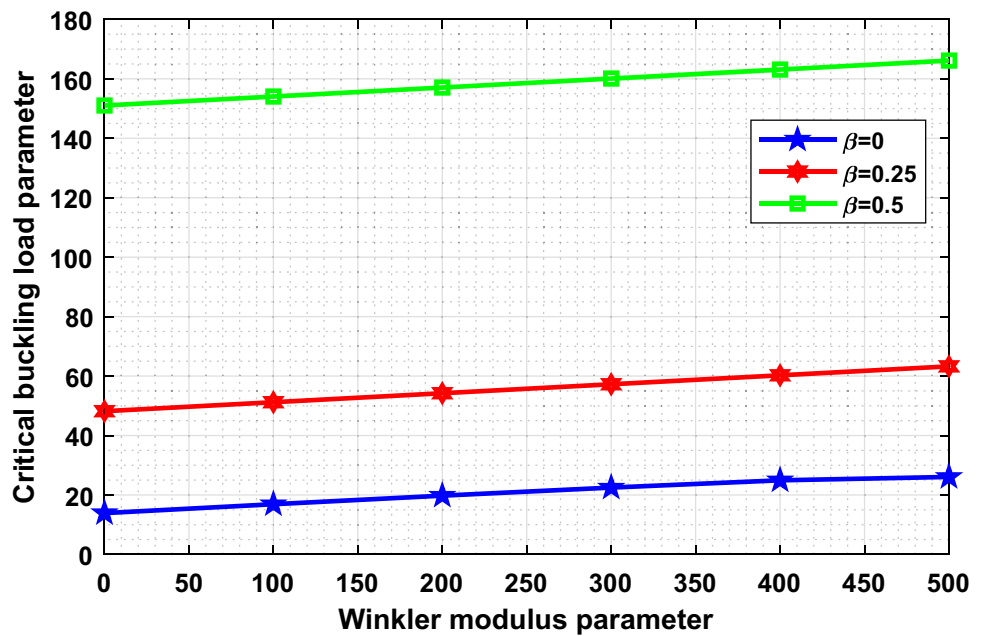
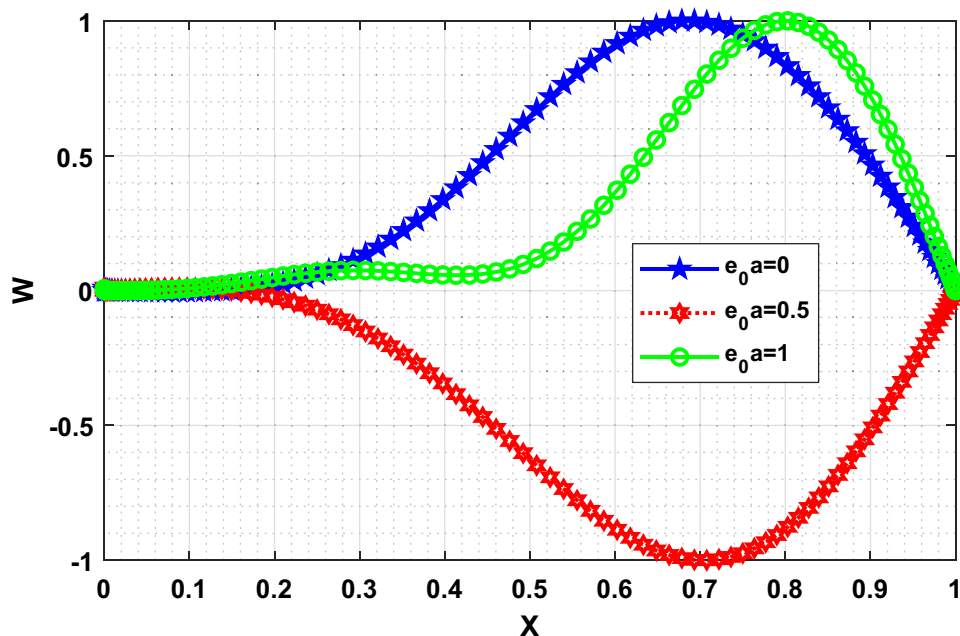


Table 4 Effect of K_w on critical buckling load parameter (\hat{P}_{cr}) by HWM, HOHWM, and DQM with $e_0a = 1$, and $L = 10$

K_w	Pinned–pinned			Clamped–clamped		
	$\hat{P}_{cr}(\beta = 0)$	$\hat{P}_{cr}(\beta = 0.25)$	$\hat{P}_{cr}(\beta = 0.5)$	$\hat{P}_{cr}(\beta = 0)$	$\hat{P}_{cr}(\beta = 0.25)$	$\hat{P}_{cr}(\beta = 0.5)$
0	4.4095	7.1295	15.2896	13.8939	48.1758	151.0215
100	9.3831	12.1031	20.2632	16.8814	51.2004	154.0474
200	14.3567	17.0767	25.2368	19.7635	54.2215	157.0724
300	17.6240	22.0503	30.2104	22.4776	57.2391	160.0965
400	18.8674	27.0239	35.1840	24.9242	60.2529	163.1197
500	20.1108	31.9975	40.1576	26.0613	63.2630	166.1420

Fig. 8 Critical buckling mode shape for PP boundary condition



condition with $K_w = 100$, $\beta = 0.2$ and $L = 10$. Mode shapes are plotted for different nonlocal parameters such as $e_0 a = 0$, $e_0 a = 0.5$ and $e_0 a = 1$ which can be seen in Fig. 8. From this figure, it is found that the critical buckling loads are affected significantly by varying different scaling parameters.

7 Concluding remarks

Buckling behavior of strain gradient nonlocal beam embedded in Winkler elastic foundation is studied using HWM, HOHWM, and DQM. The validation of the present model is conducted and found to be perfectly agreeing with the previously published article. A convergence study is also performed to exhibit the superiority of the methods. The responses of all the scaling parameters on critical buckling loads are also reported in terms of graphical and tabular results for both the boundary condition such as pinned–pinned and clamped–clamped. Followings are the main observations regarding the present investigation;

- The HOHWM and DQM are converging much faster as compared to HWM. The order of convergence of HOHWM is found to be four, whereas the order of convergence of HWM is two.
- The critical buckling loads are decreasing with an increase of nonlocal parameters for both the boundary condition and this reduction in critical buckling load is

more significant in case of clamped–clamped boundary condition.

- The critical buckling loads increase with the increase of strain gradient parameters, but this increase is much faster in case of clamped–clamped boundary conditions, and the critical buckling load is maximum in case of classical theory with higher values of strain gradient parameters, and this trend remains constant for both the boundary conditions.
- An increase in Winkler modulus parameter increases the critical buckling load for both the boundary conditions, and this increase is much higher in CC boundary condition with higher values of strain gradient parameters.

Acknowledgements The first two authors are very much thankful to the Defence Research and Development Organization (DRDO), New Delhi, India (Sanction Code: DG/TM/ERIPR/GIA/17-18/0129/020) for the funding to carry out the present research work.

References

1. Press WH, Teukolsky SA, Vetterling WT (2002) Numerical recipes in C ++: the art of scientific computing. Cambridge University Press, Cambridge
2. Murmu T, Pradhan SC (2009) Buckling analysis of a single-walled carbon nanotubes embedded in an elastic medium based on nonlocal elasticity and Timoshenko beam theory and using DQM. *Physica E* 41(7):1232–1239

3. Ansari R, Arjangpay A (2014) Nanoscale vibration and buckling of single-walled carbon nanotubes using the meshless local Petrov–Galerkin method. *Physica E* 63:283–292
4. Chakraverty S, Behera L (2016) Static and dynamic problems of nanobeams and nanoplates, 1st edn. World Scientific Publishing Co, Singapore
5. Malikan M, Jabbarzadeh M, Dastjerdi Sh (2017) Non-linear static stability of bi-layer carbon nanosheets resting on an elastic matrix under various types of in-plane shearing loads in thermo-elasticity using nonlocal continuum. *Microsyst Technol* 23:2973–2991
6. Malikan M, Sadraee Far MN (2018) Differential quadrature method for dynamic buckling of graphene sheet coupled by a viscoelastic medium using Neperian frequency based on nonlocal elasticity theory. *J Appl Comput Mech* 4:147–160
7. Golmakani ME, Malikan M, Sadraee Far MN, Majidi HR (2018) Bending and buckling formulation of graphene sheets based on nonlocal simple first order shear deformation theory. *Mater Res Express* 5:065010
8. Ansari R, Sahmani S, Rouhi H (2011) Axial buckling analysis of single-walled carbon nanotubes in thermal environments via the Rayleigh–Ritz technique. *Comput Mater Sci* 50:3050–3055
9. Jena SK, Chakraverty S (2018) Free vibration analysis of variable cross-section single layered graphene nano-ribbons (SLGNRs) using differential quadrature method. *Front Built Environ* 4:63
10. Behera L, Chakraverty S (2015) Application of differential quadrature method in free vibration analysis of nanobeams based on various nonlocal theories. *Comput Math Appl* 69:1444–1462
11. Chakraverty S, Jena SK (2018) Free vibration of single walled carbon nanotube resting on exponentially varying elastic foundation. *Curved Layer Struct* 5:260–272
12. Bakhshi Khaniki H, Hosseini-Hashemi Sh, Nezamabadi A (2018) Buckling analysis of nonuniform nonlocal strain gradient beams using generalized differential quadrature method. *Alex Eng J* 57:1361–1368
13. Chen C, Li S, Dai L, Qian C-Z (2014) Buckling and stability analysis of a piezoelectric viscoelastic nanobeam subjected to van der Waals forces. *Commun Nonlinear Sci* 19:1626–1637
14. Tuna M, Kirca M (2017) Bending, buckling and free vibration analysis of Euler–Bernoulli nanobeams using Eringen’s nonlocal integral model via finite element method. *Compos Struct* 179:269–284
15. Jena SK, Chakraverty S (2018) Free vibration analysis of single walled carbon nanotube with exponentially varying stiffness. *Curved Layer Struct* 5:201–212
16. Ghavamian A, Öchsner A (2012) Numerical investigation on the influence of defects on the buckling behavior of single- and multi-walled carbon nanotubes. *Physica E* 46:241–249
17. Jena SK, Chakraverty S, Tornabene F (2019) Vibration characteristics of nanobeam with exponentially varying flexural rigidity resting on linearly varying elastic foundation using differential quadrature method. *Mater Res Express* 6:085051
18. Jena SK, Chakraverty S, Jena RM, Tornabene F (2019) A novel fractional nonlocal model and its application in buckling analysis of Euler–Bernoulli nanobeam. *Mater Res Express* 6:055016
19. Jena SK, Chakraverty S, Tornabene F (2019) Dynamical behavior of nanobeam embedded in constant, linear, parabolic, and sinusoidal types of Winkler elastic foundation using first-order nonlocal strain gradient model. *Mater Res Express* 6:60850f2
20. Jena RM, Chakraverty S, Jena SK (2019) Dynamic response analysis of fractionally damped beams subjected to external loads using homotopy analysis method. *J Appl Comput Mech* 5:355–366
21. Jena SK, Chakraverty S (2019) Differential quadrature and differential transformation methods in buckling analysis of nanobeams. *Curved Layer Struct* 6:68–76
22. Jena SK, Chakraverty S (2018) Free vibration analysis of Euler–Bernoulli Nano beam using differential transform method. *Int J Comput Mater Sci Eng* 7:1850020
23. Jena SK, Chakraverty S, Tornabene F (2019) Buckling behavior of nanobeams placed in electromagnetic field using shifted Chebyshev polynomials-based Rayleigh–Ritz method. *Nanomaterials* 9(9):1326
24. Jena SK, Chakraverty S, Jena RM (2019) Propagation of uncertainty in free vibration of Euler–Bernoulli nanobeam. *J Braz Soc Mech Sci Eng* 41(10):436
25. Jena SK, Chakraverty S (2019) Dynamic analysis of single-layered graphene nano-ribbons (SLGNRs) with variable cross-section resting on elastic foundation. *Curved Layer Struct* 6:132–145
26. Haar A (1910) Zur Theorie der orthogonalen Funktionensysteme (German). *Mathematische Annalen* 69:331–371
27. Hariharan G, Kannan K (2013) An overview of Haar wavelet method for solving differential and integral equations. *World Appl Sci J* 23:01–14
28. Majak J, Shvartsman B, Karjust K, Mikola M, Haavajõe A (2015) On the accuracy of the Haar wavelet discretization method. *Compos Part B Eng* 80:321–327
29. Jena SK, Chakraverty S (2019) Dynamic behavior of an electromagnetic nanobeam using the Haar wavelet method and the higher-order Haar wavelet method. *Eur Phys J Plus* 134:538
30. Majak J, Pohlak M, Karjust K, Eerme M, Kurnitski J, Shvartsman BS (2018) New higher order Haar wavelet method: application to FGM structures. *Compos Struct* 201:72–78
31. Shu C (2000) Differential quadrature and its application in engineering. Springer, Berlin
32. Bert CW, Malik M (1996) Differential quadrature method in computational mechanics: a review. *Appl Mech Rev* 49:1–28
33. Tornabene F, Fantuzzi N, Ubertini F, Viola E (2015) Strong formulation finite element method based on differential quadrature: a survey. *Appl Mech Rev* 67:020801
34. Hein H, Feklistova L (2011) Free vibrations of non-uniform and axially functionally graded beams using Haar wavelets. *Eng Struct* 33:3696–3701
35. Lepik Ü (2011) Buckling of elastic beams by the Haar wavelet method. *Est J Eng* 17:271–284
36. Kirs M, Mikola M, Haavajõe A, Ounapuu E, Shvartsman B, Majak J (2016) Haar wavelet method for vibration analysis of nanobeams. *Waves Wavelets Fractals Adv Anal* 2:20–28
37. Reddy JN (2007) Nonlocal theories for bending, buckling and vibration of beams. *Int J Eng Sci* 45:288–307
38. Malikan M, Tornabene F, Dimitri R (2018) Nonlocal three-dimensional theory of elasticity for buckling behavior of functionally graded porous nanoplates using volume integrals. *Mater Res Express* 5:095006
39. Thai S, Thai HT, Vo TP, Patel VI (2018) A simple shear deformation theory for nonlocal beams. *Compos Struct* 183:262–270
40. Zhu X, Wang Y, Dai H-H (2017) Buckling analysis of Euler–Bernoulli beams using Eringen’s two-phase nonlocal model. *Int J Eng Sci* 116:130–140
41. Tuna M, Kirca M (2016) Exact solution of Eringen’s nonlocal integral model for vibration and buckling of Euler–Bernoulli beam. *Int J Eng Sci* 107:54–67
42. Thai H-T (2012) A nonlocal beam theory for bending, buckling, and vibration of nanobeams. *Int J Eng Sci* 52:56–64
43. Malikan M (2017) Electro-mechanical shear buckling of piezoelectric nanoplate using modified couple stress theory based on simplified first order shear deformation theory. *Appl Math Model* 48:196–207

44. Akgöz B, Civalek Ö (2012) Free vibration analysis for single-layered graphene sheets in an elastic matrix via modified couple stress theory. *Mater Design* 42:164–171
45. Nematollahi MS, Mohammadi H (2019) Geometrically nonlinear vibration analysis of sandwich nanoplates based on higher-order nonlocal strain gradient theory. *Int J Eng Sci* 156:31–45
46. Malikan M, Nguyen VB, Tornabene F (2018) Damped forced vibration analysis of single-walled carbon nanotubes resting on viscoelastic foundation in thermal environment using nonlocal strain gradient theory. *Eng Sci Technol Int J* 21:778–786
47. Malikan M, Dimitri R, Tornabene F (2019) Transient response of oscillated carbon nanotubes with an internal and external damping. *Compos Part B Eng* 158:198–205
48. Wang J, Shen H, Zhang B, Liu J, Zhang Y (2018) Complex modal analysis of transverse free vibrations for axially moving nanobeams based on the nonlocal strain gradient theory. *Physica E* 101:85–93
49. She GL, Yan KM, Zhang YL, Liu HB, Ren YR (2018) Wave propagation of functionally graded porous nanobeams based on non-local strain gradient theory. *Eur Phys J Plus* 133:368
50. Mehralian F, Tadi Beni Y, Karimi Zeverdejani M (2017) Nonlocal strain gradient theory calibration using molecular dynamics simulation based on small scale vibration of nanotubes. *Physica B* 514:61–69
51. Malikan M, Nguyen VB, Dimitri R, Tornabene F (2019) Dynamic modeling of non-cylindrical curved viscoelastic single-walled carbon nanotubes based on the second gradient theory. *Mater Res Express* 6:075041
52. Zhu X, Li L (2017) Closed form solution for a nonlocal strain gradient rod in tension. *Int J Eng Sci* 119:16–28
53. Zhu X, Li L (2017) On longitudinal dynamics of nanorods. *Int J Eng Sci* 120:129–145
54. Tang H, Li L, Hu Y, Meng W, Duan K (2019) Vibration of nonlocal strain gradient beams incorporating Poisson's ratio and thickness effects. *Thin-Walled Struct* 137:377–391
55. Li L, Tang H, Hu Y (2018) The effect of thickness on the mechanics of nanobeams. *Int J Eng Sci* 123:81–91
56. Li L, Hu Y (2015) Buckling analysis of size-dependent nonlinear beams based on a nonlocal strain gradient theory. *Int J Eng Sci* 97:84–94
57. Lim CW, Zhang G, Reddy JN (2015) A higher-order nonlocal elasticity and strain gradient theory and its applications in wave propagation. *J Mech Phys Solids* 78:298–313
58. Khaniki HB, Hosseini-Hashemi S (2017) Buckling analysis of tapered nanobeams using nonlocal strain gradient theory and a generalized differential quadrature method. *Mater Res Express* 4:065003
59. Li L, Hu Y (2015) Buckling analysis of size-dependent nonlinear beams based on a nonlocal strain gradient theory. *Int J Eng Sci* 97:84–94
60. Li L, Li X, Hu Y (2016) Free vibration analysis of nonlocal strain gradient beams made of functionally graded material. *Int J Eng Sci* 102:77–92
61. Li L, Hu Y (2017) Post-buckling analysis of functionally graded nanobeams incorporating nonlocal stress and microstructure-dependent strain gradient effects. *Int J Eng Sci* 120:159–170
62. Karami B, Shahsavari D, Li L (2018) Hygrothermal wave propagation in viscoelastic graphene under in-plane magnetic field based on nonlocal strain gradient theory. *Physica E* 97:317–327
63. Sahmani S, Fattahi AM, Ahmed NA (2019) Analytical mathematical solution for vibrational response of postbuckled laminated FG-GPLRC nonlocal strain gradient micro-/nanobeams. *Eng Comput* 35:1173–1189
64. Ebrahimi F, Barati MR, Civalek Ö (2019) Application of Chebyshev–Ritz method for static stability and vibration analysis of nonlocal microstructure-dependent nanostructures. *Eng Comput*. <https://doi.org/10.1007/s00366-019-00742-z>
65. Ebrahimi F, Karimiasl M, Mahesh V (2019) Chaotic dynamics and forced harmonic vibration analysis of magneto-electro-viscoelastic multiscale composite nanobeam. *Eng Comput*. <https://doi.org/10.1007/s00366-019-00865-3>
66. Malikan M, Nguyen VB (2018) Buckling analysis of piezo-magneto-electric nanoplates in hygrothermal environment based on a novel one variable plate theory combining with higher-order nonlocal strain gradient theory. *Physica E* 102:8–28
67. Malikan M, Nguyen VB, Tornabene F (2018) Electromagnetic forced vibrations of composite nanoplates using nonlocal strain gradient theory. *Mater Res Express* 5:075031
68. Malikan M, Dimitri R, Tornabene F (2018) Effect of sinusoidal corrugated geometries on the vibrational response of viscoelastic nanoplates. *Appl Sci* 8:1432
69. Chen CF, Hsiao CH (1997) Haar wavelet method for solving lumped and distributed-parameter systems. *IEE Proc Control Theory Appl* 144:87–94
70. Lepik U (2012) Exploring vibrations of cracked beams by the Haar wavelet method. *Estonian J Eng* 18:58
71. Quan JR, Chang CT (1989) New insights in solving distributed system equations by the quadrature method—I. Analysis. *Comput Chem Eng* 13:779–788
72. Quan JR, Chang CT (1989) New insights in solving distributed system equations by the quadrature method—II. Numerical experiments. *Comput Chem Eng* 13:1017–1024
73. Majak J, Shvartsman BS, Kirs M, Pohlak M, Herranen H (2015) Convergence theorem for the Haar wavelet based discretization method. *Compos Struct* 126:227–232
74. Kirs M, Eerme M, Bassir D, Tungel E (2019) Application of HOHWM for vibration analysis of nanobeams. *Key Eng Mater* 799:230–235
75. Wang CM, Zhang YY, Ramesh SS, Kitipornchai S (2006) Buckling analysis of micro- and nano-rods/tubes based on nonlocal Timoshenko beam theory. *J Phys D* 39:3904
76. Shvartsman BS, Majak J (2016) Numerical method for stability analysis of functionally graded beams on elastic foundation. *Appl Math Model* 40:3713–3719

Publisher's Note Springer Nature remains neutral with regard to jurisdictional claims in published maps and institutional affiliations.